An Application of 3-D MEMS Packaging: Out-of-Plane Quadrupole Mass Filters

Luis F. Velásquez-García, Kerry Cheung, and Akintunde I. Akinwande

***Abstract*—This paper reports the design, fabrication, and characterization of low-cost out-of-plane quadrupole mass filters that use commercially available dowel pins as electrode rods. The quadrupoles implement a 3-D MEMS packaging technology that relies on deep-reactive ion etching (DRIE)-patterned deflection springs for alignment. Quadrupoles with rod diameter ranging from 0.25 to 1.58 mm and aspect ratio of 30 to 60 were built and tested at RF frequencies of 1.44, 2.0, and 4 MHz. Assembled devices operated in the first stability region achieved a maximum mass range of 650 amu, while a minimum half-peak width of 0.4 amu at mass 28 was obtained in the second stability region. Operation in the second stability region provides a means to higher resolution, smoother peaks, and removed peak splitting at the expense of transmission. The ultimate resolution of the reported quadrupoles is also discussed. [2008-0060]**

***Index Terms*—Mass filter, out-of-plane quadrupole, second stability region, 3-D packaging.**

I. Introduction

A QUADRUPOLE is an apparatus comprising of four electrodes arranged in a symmetric manner that can filter charged species if driven with a mix of constant and time-varying electric potentials [1]. Quadrupole, ion trap, and magnetic sector mass filters all separate ions according to their mass-to-charge ratios, but quadrupoles are the most popular due to their simple design and usage. Development of scaled-down quadrupoles has been an active area of interest in the past decade. The motivation behind this effort is driven by the desire for rugged gas chromatography and mass spectrometry (GC/MS) systems that are smaller, lighter, cheaper, faster, and more power efficient [2]–[4]. The successful implementation of portable GC/MS systems would significantly impact areas such as law enforcement, geological analysis, environmental monitoring, and space exploration [5]–[7].

Scaling-down quadrupoles poses several advantages for mass spectrometers—portability, reduced cost, high-pressure operation, and lowered power consumption. A decrease in the size and weight of the mass filter will reduce overall material costs, and serve as a step toward portability. Miniaturized drive electronics, ionizers, detectors, as well as a viable pumping scheme need to be addressed before truly portable mass spectrometers can be realized. The most problematic component is the pump but scaled-down mass filters will relax vacuum requirements, enabling high-pressure operation and facilitating the development and use of a low-powered pumping strategy [8].

Despite these potential advantages, miniaturization of quadrupoles results in reduced transmission, demanding assembly precision, and increased drive-circuit complexity. The loss of transmission can be recovered by operating at higher pressures and/or the use of quadrupole arrays [9]. An assembly precision of 0.2% of the rod diameter is reported to give a resolution of 200 over a 100-amu mass range [9] while a misalignment of $> 1\%$ of the nominal rod diameter has been stated to result in a severe decrease in device performance [10]. Advances in machining techniques and the inherent precision of microfabrication technology make it possible to meet these tolerances. The shortening of quadrupole lengths will require higher RF drive frequencies for suitable resolution, while the resulting decrease in capacitance (see the Appendix) will lead to dominating parasitics. These two issues contribute to reduced power efficiency and a need for innovative drive-circuit designs.

Several groups have scaled-down quadrupole mass filters by using conventional manufacturing technologies. The Jet Propulsion Laboratory (Pasadena, CA) and Thorleaf Research (Santa Barbara, CA) have been developing a miniaturized GC/MS for space flight missions. Their device comprises of a quadrupole array that utilizes various precision-machined ceramics and components [8], [11], [12]. Inficon (East Syracuse, NY) has developed miniature quadrupole residual gas analyzers (RGAs) that are milled with electrical discharge machining [13]. Ion Metrics (San Diego, CA) has a miniaturized RGA that uses a quadrupole array and a thermionic ion source [14]. Their RGA is produced using a technology similar to what is used to manufacture vacuum tubes. Although practical, these engineering processes are all relatively expensive.

Microfabricated mass filters have been developed as alternatives to miniaturized quadrupoles in attempts to address costs. Syms *et al.* [15]–[17] have worked on two in-plane MEMS quadrupole concepts. The first used KOH grooves to guide the assembly of metallized glass rods, while the second uses deep-reactive ion etching (DRIE) springs patterned on an SOI stack to align and hold the electrodes [18]. Verbeck *et al.* [19] demonstrated a MEMS ion trap mass filter which also used DRIE spring technology, but precision robotics were required for assembly. Sillon and Baptist [20] developed a Wien filter for helium detection that had modest performance for low-mass detection but was limited in resolution at higher masses.

Manuscript received March 7, 2008; revised August 29, 2008. Current version published December 4, 2008. This work was supported by DARPA/MTO and the U.S. Army Soldier Systems Center (Natick, MA) under Contract W911QY-05-1-0002 (DARPA program managers C. Nguyen and D. Polla, and Army program manager H. Girolamo). Subject Editor D. L. DeVoe.

The authors are with the Massachusetts Institute of Technology, Cambridge, MA 02139 USA (e-mail: lfvelasq@mit.edu; cheung@mit.edu; akinwand@mtl.mit.edu).

Digital Object Identifier 10.1109/JMEMS.2008.2006769

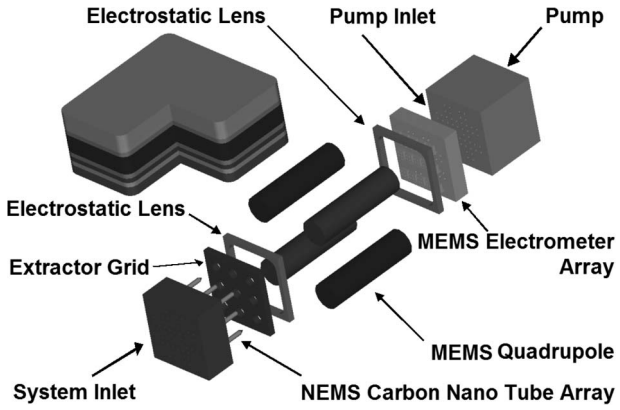

Fig. 1. System architecture of a MEMS-based portable mass spectrometer sensor.

Wiberg *et al.* [21] reported a MEMS quadrupole array of copper electrodes formed from LIGA but no data were presented.

This paper reports a cost-effective MEMS out-of-plane quadrupole mass filter developed as part of a portable gas analyzer system. The proposed system architecture includes a carbon nanotube-based ionizer array [22], an array of MEMS electrometers for species detection [23], and a MEMS vacuum pump in addition to the mass filter (Fig. 1). The quadrupole implements a 3-D MEMS packaging technology that relies on DRIE patterned deflection springs to aid the hand-assembly of subcomponents with precision on the order of a few micrometers [24]. The out-of-plane fashion of these MEMS quadrupoles comes from integration considerations to the MEMS ion sources and MEMS detectors developed for the system. The use of the second stability region to improve performance in microfabricated quadrupoles is demonstrated, and the results are discussed. Section II of this paper gives a brief introduction to quadrupole performance, and Section III describes the design and fabrication of the μGripper quadrupoles. Section IV addresses the experimental setup and test methodology, while the experimental results of the proposed quadrupole technology are discussed in Section V.

II. Quadrupole Performance

Quadrupole fields and their application in MS have been studied for some time, and the theory of operation is readily available in the scientific literature [25], [26]. From the operating principles, there are two main indicators of quadrupole performance—the resolution and the mass range. The principal figure of merit is the resolution, which gives an indication of how well mass peaks can be distinguished from peaks arising from adjacent masses. A large value for the resolution implies the quadrupole will be able to differentiate masses more precisely. The mass range is simply the maximum mass resolvable for a given set of operating conditions. This value is typically limited by the electrical breakdown of the device and the driving electronics.

Ideal quadrupoles use hyperbolic electrodes but most commercially available versions use circular rods instead for their manufacturing simplicity. The majority of researchers report that quadrupoles with circular electrodes of radius r perform the best if the rods are tangential to a circle of radius $r_{\rm o}$ with an $r - to - r_{\rm o}$ ratio of 1.148. This value originated from work on magnetic quadrupoles [27], [28] and was later revised by Denison [29]. Recent work using more accurate simulation techniques report optimal ratios that are noticeably different [30], [31]. Despite this optimization, the use of circular rods results in precursors that degrade peak shape and resolution [32]. Precursors peaks arise from unwanted field components that are a result of using nonhyperbolic electrodes. Nonidealities such as rod misalignment, fringing fields, high ion energies, and poor ion optics will also contribute to reduced performance.

The dynamics of a charged particle within a hyperbolic field are described by the Mathieu equation which has stable and unstable solutions. These solutions can be mapped, defining stability regions which correspond to sets of operating conditions that permit stable ion trajectories. The majority of work on linear quadrupoles uses the first stability region, but some researchers have investigated the second stability region for the increased resolution at a given RF frequency [33], [34]. The quadrupole resolution R is defined as

$$R = m/\Delta m \tag{1}$$

where Δm is the width of the peak centered around mass m. Several definitions of peak width are used in the literature, but this paper will use the peak full-width at half-maximum (FWHM). It has been shown experimentally that resolution is proportional to the square of the number of RF cycles n that a charged particle spends within the quadrupole

$$R \cong n^2/h \tag{2}$$

where h is a constant dependent on the stability region and experimental setup. Typical values for h of 10 to 20 have been found for the first stability region, and 0.73 to 1.43 for the second stability region [25].

From a simple physical argument, the number n can be expressed as

$$n = f \cdot \frac{L}{v_z} = f \cdot L\sqrt{\frac{m}{2 \cdot E_z}} \tag{3}$$

where m is the charged particle mass, f is the RF frequency, L is the length of the quadrupole, and v_z is the axial speed of the charged particle with an axial energy E_z. Clearly, an increased frequency will lead to improved resolution but if all else remains constant, drive voltages will need to be increased accordingly to maintain the operating point. Decreasing the rod diameter can offset this increase, supporting the feasibility of small quadrupoles that performs just as well as larger ones at the expense of increased frequency and stronger electric fields. Combining (2) and (3), the resolution can be expressed as

$$R \cong \frac{f^2 \cdot L^2 \cdot m}{2 \cdot E_z \cdot h}. \tag{4}$$

From (4) and the h values reported by Dawson [25], it can be seen that a quadrupole operated in the second stability region will have better resolution than a quadrupole operated in the first stability region with all else constant. In this case, the

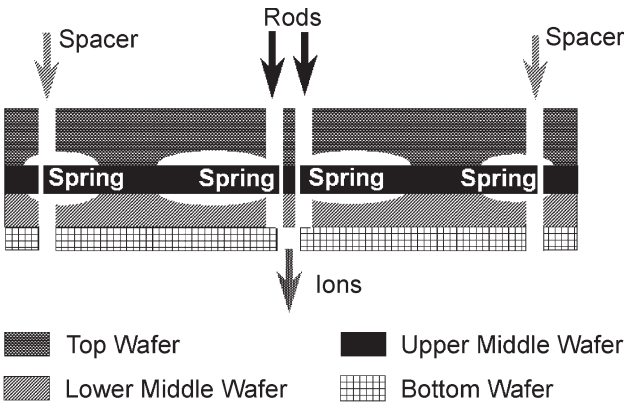

Fig. 2. μGripper cross section.

increase in resolution is given by the ratio h_1/h_2, where h_1 is the h value for the first stability region and h_2 is the h value for the second stability region. Gauss' law of error propagation states that the maximum uncertainty ΔF of a function $F(x_1, x_2, \ldots, x_n)$ evaluated at $X = (X_1, X_2, \ldots, X_n)$ due to the uncertainties $(\Delta X_1, \Delta X_2, \ldots, \Delta X_n)$ is given by [35]

$$\Delta F \cong \sqrt{\sum_{i=1}^{n} \left(\left. \frac{\partial F}{\partial x_i} \right|_X \cdot \Delta X_i \right)^2}. \tag{5}$$

If (5) is used with $F = h_1/h_2$, $h_1 = 15 \pm 5$, and $h_2 = 1.08 \pm 0.35$, it is concluded that operating a quadrupole in the second stability region can give a 7 to 20 fold increase in resolution compared to a quadrupole operated in the first stability region. This improvement comes with a significant reduction in transmission and the need for larger RF and dc voltages to scan the same mass range.

III. Device Design and Fabrication

The μGripper is a microfabricated platform that uses silicon DRIE-patterned deflection springs to aid the hand-assembly of out-of-plane MEMS quadrupoles. A 3 cm $\times$ 3 cm square with spacer holes near the corners and electrode holes near the center, this flexible platform can accommodate 0.25- to 1.58-mm diameter rods with any aspect ratio. The electrode holes are placed so the $r - to - r_o$ ratio is the commonly used value of 1.148. Fig. 2 shows a cross section that depicts the four silicon layers that make up the device. The core of the μGripper is the Upper Middle Wafer that has the deflection springs. The Top and Lower Middle Wafers are mirror images except that the top wafer is thicker. These two wafers have recesses that surround the deflection springs to ensure smooth actuation, and through holes for the quadrupole rods and spacers. The Bottom Wafer has a set of through holes for ion transmission and the spacer assembly. This assembly technology has an average rms biaxial misalignment of 6.2 ± 0.6 μm, an average in-plane angular misalignment of $1.7 \pm 0.5'$, and an average out-of-plane angular misalignment of $0.14 \pm 0.45^\circ$ [24], [36].

An assembled MEMS quadrupole with 250-μm diameter rods along with a schematic cross section is shown in Fig. 3. The quadrupole assembly has three microfabricated pieces: a top aligning plate, an exit lens, and the μGripper. The inlet lens was manufactured with conventional machining since it was simpler and cheaper than using microfabrication techniques. Kapton washers, metallic spacers, and commercial dowel pins with 5-μm precision in diameter are also needed to complete the quadrupole assembly. Factoring in the precision of the dowel pins, the assembled devices will have an average rod misalignment of about 9.1 μm.

Two generations of the μGripper have been developed with the second improving on issues discovered after characterization of the original. The first generation had two springs per electrode with each spring controlling a different axis, while the second only has one (Fig. 4). During assembly, the electrodes will experience axial compression from the applied force and the spring restoring force which can lead to buckling and permanent deformation if the rod diameter is too small. Quadrupoles with an aspect ratio of 30 and rod diameter of 550 μm were successfully built with the first generation μGripper [37]. In the second generation, highly doped substrates were used to improve device performance by ensuring equipotential surfaces, while a silicon-rich nitride coating was deposited to prevent scratching of the springs during assembly. Additionally, the structure included spring tip handlers that would retract the spring during rod insertion to eliminate the possibility of buckling. Quadrupoles with various lengths and rod diameters of 0.25, 0.55, 1.0, and 1.58 mm were constructed with the second generation μGripper.

The microfabricated components of the quadrupoles were made at MIT's Microsystems Technology Laboratories. One process flow was used to produce the top aligning plates and electrostatic lenses, and another for the μGrippers. The process flows of the first and second generation μGrippers are almost identical with two key differences. The original used wafers lightly doped with boron, while the newer version uses wafers highly doped with antimony. The second generation also includes a 1-μm silicon-rich nitride low-pressure chemical vapor deposition layer after the final oxidation to serve as a scratch barrier.

A. Plate/Lens Process Flow

The aligning plates use 1000 ± 5-μm-thick substrates, while the lenses use 500 ± 5-μm-thick substrates. The wafers are spin coated with thick resist on one side, and the patterns for the aligning plates/electrostatic lenses are transferred with contact photolithography. The wafers are mounted onto a quartz handle wafer, patterned with a through wafer DRIE to form the components, and dismounted using an acetone soak. The aligning plates are RCA cleaned and covered with 2 μm of thermal oxide, while the electrostatic lenses are piranha cleaned and sputtered on both sides with 1 μm of Al and a 100-nm Ti adhesion layer.

B. First Generation μGripper Process Flow

The μGripper consists of the Top and Upper Middle Wafers which are 1000 ± 5 μm thick, and the Lower Middle and Bottom Wafers which are 500 ± 5 μm thick. All these layers begin with an RCA clean and a thermal oxide growth of 0.3 μm in order to protect the bonding surfaces. Alignment marks are

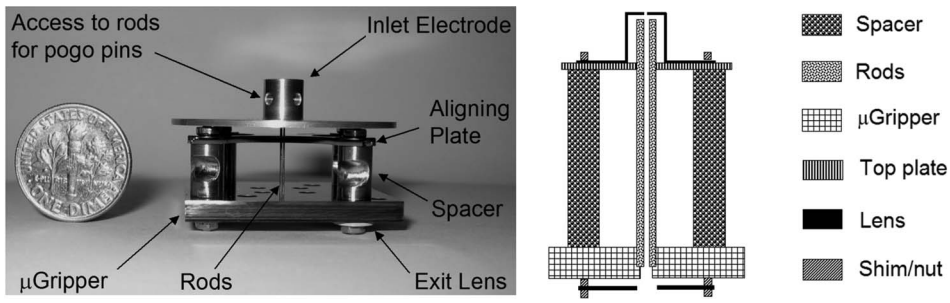

Fig. 3. (Left) Fully assembled μGripper quadrupole with 250-μm diameter rods and aspect ratio of 60. (Right) Schematic cross section.

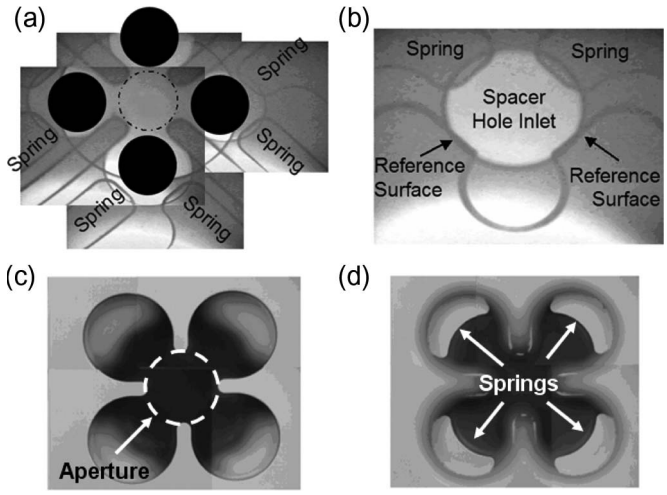

Fig. 4. IR images of the first-generation μGripper: (a) springheads for the (dark circles) electrodes surrounding the (dotted circle) aperture and (b) springheads for the metallic spacers. Microscope images of the second-generation μGripper: (c) reference surfaces and aperture and (d) springheads for the electrodes (one per electrode).

defined on both sides through the use of thin resist with contact photolithography, followed by a reactive ion etch (RIE) of the oxide and silicon. The resist is stripped with piranha, 4 μm of plasma-enhanced chemical vapour deposited (PECVD) oxide is deposited on one side to serve as a hard mask, and then the wafers are annealed at 950 °C for 1 h in nitrogen. Subsequent process steps are as follows.

1) *Top Wafer/Lower Middle Wafer* [Fig. 5(a)]: Both sides of the wafers are coated with thick resist and exposed using contact photolithography. The resist on the PECVD oxide is patterned with through holes for the rods, spacers, and transmission zone, while the resist on the other side is patterned with the recesses that surround the deflection springs. The oxide on both sides is patterned with RIE, and the 5-μm-deep recesses are etched into the silicon using SF_6. The wafers are flipped, attached to a quartz handle wafer, and the through holes are etched using DRIE.
2) *Upper Middle Wafer/Bottom Wafer* [Fig. 5(b)]: The side with the PECVD oxide is coated with thick resist and exposed using contact photolithography. The Upper Middle Wafer is patterned with the deflection springs, while the Bottom Wafer is patterned with the spacer and transmission through holes. The PECVD oxide is etched with RIE, the wafers are mounted onto a quartz handle wafer, and the patterns are etched with a through wafer DRIE.
3) *Final Processing* [Fig. 5(c)]: The wafers are dismounted using acetone, cleaned with piranha, then stripped of their oxide in a 49% HF bath. The wafers are RCA cleaned, aligned, bonded at atmosphere, and pressed with 2500 N for at least 12 h. The bonded stack is then annealed at 1050 °C for 1 h in nitrogen, followed by 2 μm of thermal oxide growth and then die sawing.

IV. Experimental Setup and Test Methodology

The experimental setup consists of a custom made rig to hold and contact the quadrupole electrodes, a thermionic ionizer from Ardara Technologies (Ardara, PA), associated ion optics, and a Channeltron dynode detector, all placed into a high vacuum system (Fig. 6). The chamber has an inlet valve which allows the introduction of air or perfluorotributylamine (FC-43), a standard calibration compound. RF and dc power are fed into the chamber through low-capacitance coaxial cables and a bias-tee circuit, while the detector signal is magnified by a preamplifier and recorded. The entire setup is monitored by a Merlin automation data system that has a 12.5-kHz data acquisition board, and controllers made by Extrel (Pittsburgh, PA). Merlin provides power and control to numerous components of the setup making optimization and data acquisition relatively straightforward. Parameters such as lens voltages, ion energy, detector gain, scan rates, and many others can be changed on the fly.

DC power was supplied by the Merlin box while three different power supplies were available for the RF. These supplies have a fixed dynamic range greater that what was needed in our experiments so resistive and capacitive voltage dividers were used to step them down accordingly. A RF supply from Pfeiffer Vacuum (Nashua, NH) was operated at 1.44 MHz, while the other two from Ardara Technologies were operated at 2.0 and 4 MHz. The RF supplies are self-resonating so they tune automatically with the capacitive load presented by the quadrupole, parasitics, and passive components in the bias-tee network. A tuning capacitor was used to correct for frequency shifts arising from modifications in the overall circuit, including the changing of quadrupoles.

For each quadrupole to be tested, calculations were made to determine the voltages required to scan a desired mass range at the available frequencies in stability regions I and II. To

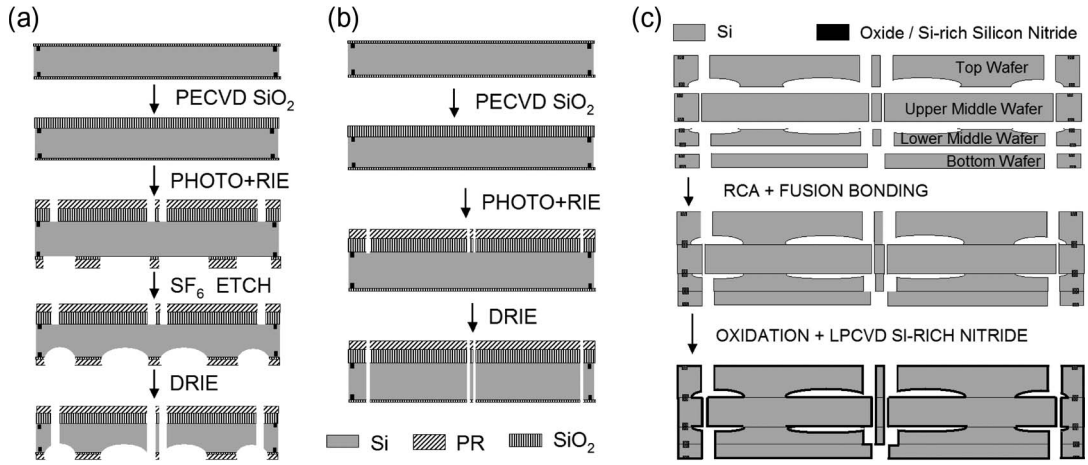

Fig. 5. Process flow schematics. (a) Top wafer and lower middle wafer. (b) Upper middle wafer and bottom wafer. (c) Final steps for the μGripper.

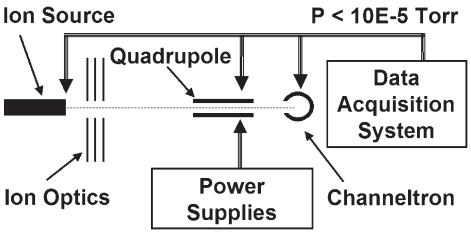

Fig. 6. Experimental setup.

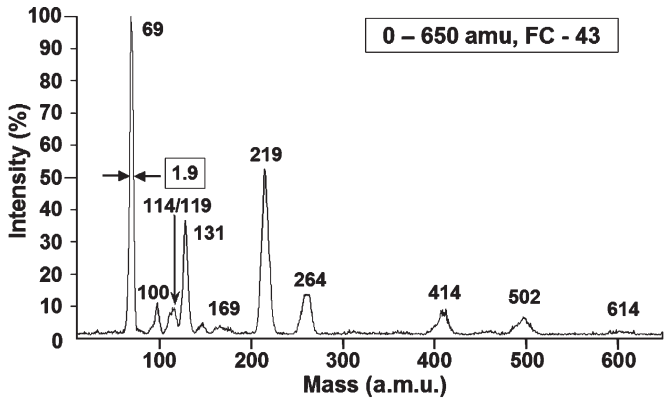

Fig. 7. FC-43 spectrum: 1.44 MHz, 1.58-mm rods, ion energy 13.6 eV, scan rate 323 amu/s.

prevent electrical breakdown of the devices, a maximum peak-to-peak voltage of 150 V was imposed, even though breakdown was experimentally determined to be 800 V. Starting with the quadrupole with the largest rod diameter, testing was conducted in a progressive manner to explore the limits of this technology. FC-43 is used to determine the mass range detectable due to its broad range of peaks, while air is used to determine the maximum resolution due to its closely spaced peaks. Operation in the second stability region was explored as a way to improve the resolution.

The experimental procedure begins with placing the assembled quadrupoles into the custom testing rig, aligning the detector, ionizer, and optics, and making connections to the corresponding electronics. The entire structure is loaded into the vacuum chamber and held until $< 10^{-6}$ torr is reached. Either air or FC-43 is introduced into the chamber and stabilized at a pressure of $\sim 10^{-5}$ torr before the ionizer is turned on. RF power is applied, the circuit is tuned, and adjustments are made to the RF and dc supplies to set the calculated voltages. A mass range and scan rate is initially selected and minor adjustments are made to the drive voltages until a signal appears, followed by optimization of the lens voltages to improve the signal strength. Once this is established, more adjustments are made through the Merlin system to improve peak shape by changing the scan rate, the pole bias voltage, and the ion energy. The scanned data are averaged 100 times to minimize noise, and the detected peaks are calibrated against the known peaks of FC-43 or air. Once the desired spectra are collected, the Merlin system is turned off along with all the electronics, the flow of the calibration substance is stopped, and the system is allowed to cool before venting.

V. Results and Discussion

A quadrupole with 1.58-mm rods and an aspect ratio of 57 was tested at 1.44 MHz with FC-43 to generate an initial spectrum. The same device was then tested at 2.0 and 4 MHz with air to demonstrate improvements in resolution. Fig. 7 shows a mass range of 650 amu, a peak width of 1.9 amu at peak 69, and a width of 2.2 amu at mass 219. These data illustrate a resolution of $\sim$100, and supports the claim that the Merlin system operates in a constant peak-width mode [38]. The peak widening at the larger masses can be attributed to the ultimate resolution of the quadrupole being reached. Operation at higher frequencies exhibits narrower peak widths, as shown in Figs. 8 and 9, but issues with peak shape are much more apparent. The spectra expose small precursor peaks on the low-mass side and minor peak splitting on the high-mass side that are worse in the 2.0 MHz data, indicating better performance at higher driving frequencies. Precursors are associated with the use of circular rods, while the peak splitting is attributed to nonidealities such as misalignment and the fundamental periodic nature of the ion trajectories [39]. Other than the slight peak shift of monatomic oxygen in Fig. 8, these spectra show good agreement with the library spectra of FC-43 and air. The shift observed is likely due to tuning issues of the Merlin system or the nonlinearity of the RF supply at the low end of its amplitude range.

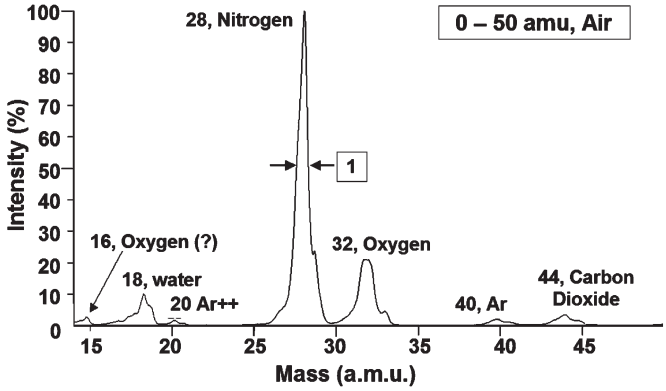

Fig. 8. Air spectrum: 2.0 MHz, 1.58-mm rods, ion energy 13.6 eV, scan rate 250 amu/s.

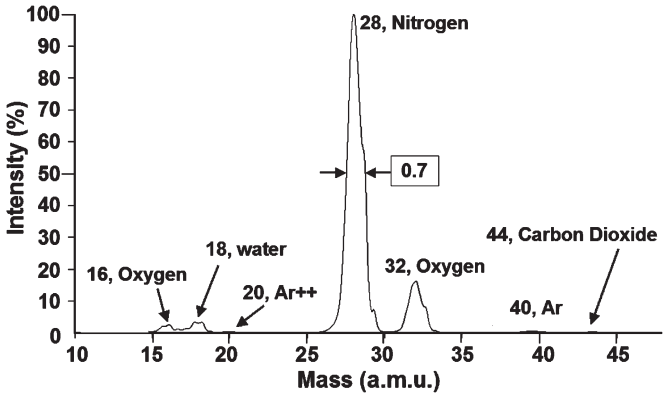

Fig. 9. Air spectrum: 4 MHz, 1.58-mm rods, ion energy 13 eV, scan rate 125 amu/s.

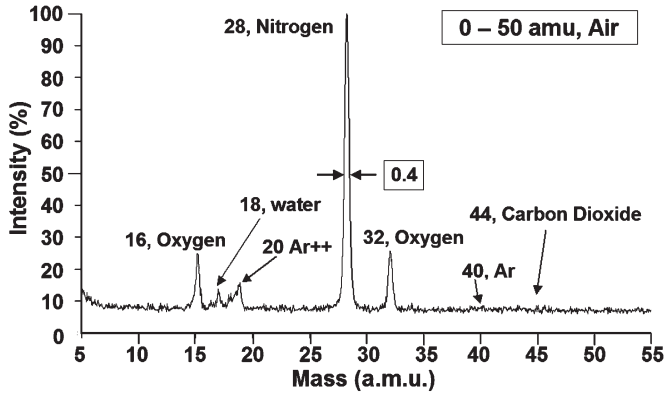

Fig. 10. Air spectrum: 2.0 MHz, 1.58-mm rods, ion energy 60 eV, scan rate 125 amu/s, second stability region.

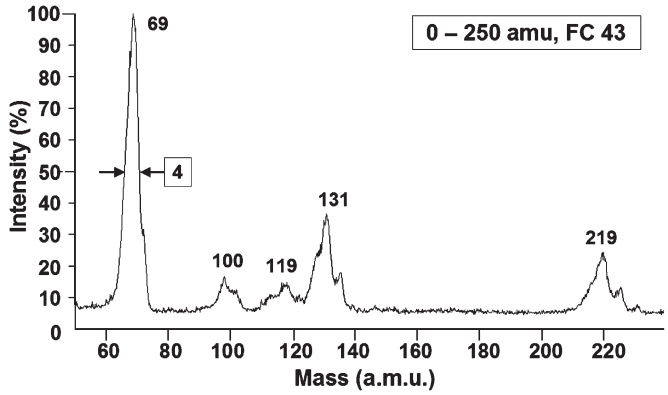

Fig. 11. FC-43 spectrum: 4 MHz, 1.0-mm rods, ion energy 40 eV, scan rate 250 amu/s.

Under constant peak width operation, we can infer that the peak width for N_2 at 1.44 MHz will be approximately 1.9 amu, thus giving a resolution of ∼15. With this assumption and (4), we predict a resolution of ∼29 for N_2 at 2.0 MHz which is in good agreement with the measured value of ∼28. Utilizing the same scaling law, a resolution of ∼118 is expected at 4 MHz but only a resolution of ∼40 was measured. A possible explanation is given by Titov [40], who concluded that at high RF frequencies, resolution is proportional to the number of cycles spent in the quadrupole to the 4/3 power. This conclusion would modify (4), resulting in a lower than expected resolution as observed.

For operation in the second stability region, a driving frequency of 2.0 MHz was used instead of 4 MHz to prevent exceeding the voltage limits. The spectrum in Fig. 10 exhibits smooth near-symmetric peaks without precursors or peak splitting, but the transmission is significantly reduced. The signal-to-noise ratio (SNR) of the measurements in the first stability region is greater than 100, but is reduced by a factor of 10 in the second stability region. One way to compensate for this loss is to match the ionizer emittance to the quadrupole acceptance through the use of ion optics and appropriately sized inlet apertures. This matching will optimize transmission, but space charge effects arising from focused ions may diminish the benefits. In the second stability region, fringing fields at the inlet are strongly defocusing which contributes to the decreased transmission [33]. In order to overcome these nonidealities inherent in the experiment, an ion energy of 60 eV was used. This high energy reduces the residence time of the ion in the quadrupole so the resolution suffers to a degree. From the range of h values in the literature and the ion energies used, the resolution expected is a 1.6 to 4.6 fold increase from that shown in Fig. 8. A 2.5-fold improvement was measured which is consistent with calculated values.

Proceeding onto smaller quadrupoles, a 1.0-mm device with an aspect ratio of 37 was driven at 4 MHz with FC-43 as the analyte. Fig. 11 exhibits a peak width of 4 amu at mass 69 corresponding to a resolution of ∼18. Using (4) modified by Titov's argument for high-frequency operation, data from Fig. 9, and the experimental parameters, a resolution of ∼11 is expected which is on the order of what was measured. Once again, high ion energies were needed to overcome the fringing field effects. In this case, they have become more prominent due to the smaller rod dimensions. Fringing fields play a crucial role at the inlet since they modify the initial position and velocity of the ions, leading to drastic changes in the ion dynamics. Effects at the outlet, where the μGripper contacts the electrodes, are of minimal consequence since exiting ions are swept into the detector from the large negative bias applied to it. The SNR for this data is comparable to that shown in Fig. 10, but the reduction in transmission observed, in this case, is mainly due to the overall decrease in aperture size associated with a smaller

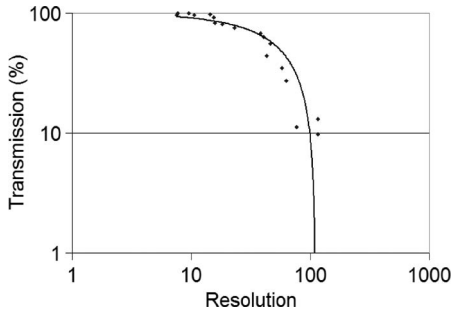

Fig. 12. Transmission versus resolution, 4 MHz, 1.0-mm rods, FWHM of peaks at 69 amu.

device. The peak splitting and noding seen can be attributed to the relative increases in rod misalignment due to scaling down.

Driving the 1.0-mm device in the second stability region was unable to produce any data. The additional reduction in transmission that comes with operating in the second stability region made it unfeasible to obtain peaks above the noise floor of the current test setup. The results of this experiment led to the conclusion that the 0.55- and 0.25-mm devices would also be unlikely to produce significant data. Improved ion optics and quadrupole inlet conditions can eliminate the use of high ion energies, while better detectors can decrease the noise floor. Having these improvements can potentially pave a way to the testing of the smaller devices.

To determine the ultimate resolution of the assembly technology, a transmission versus resolution plot was generated for the 1.0-mm device using mass 69 of FC-43 (Fig. 12). From the transmission versus resolution curve, we see that the quadrupole technology gives an ultimate resolution of $\sim$125 for the 1.0-mm device. If we take the ratio between the rod diameter and the average rod misalignment of 9.1 μm, we get $\sim$110, close to the ultimate resolution measured. Applying the same technique to the larger quadrupole, we would expect an ultimate resolution of $\sim$170 which is consistent with the data in Fig. 7. This *ad hoc* calculation seems to hold true for the ultimate resolution of macroscaled quadrupoles as well [41]. This misalignment corresponds to $\sim$0.9% the rod diameter, potentially causing the peak shapes observed since it is on the high end of what is tolerable. With this data set, an estimated sensitivity of 5×10^{10} counts/torr $\cdot$ s including the detector gain of 1000 was calculated.

These experimental results are encouraging since they show satisfactory device performance with good correlation to analytical values. The reported device technology demonstrates a mass range of 650 amu, a maximum resolution on the order of 125, and a minimum peak width of 0.4 amu. The miniaturized RGA from Ion Metrics (San Diego, CA) has a mass range of 300 amu and peak widths of 1.5 amu, while the best performing MEMS quadrupole previously published reports a mass range of 400 amu, a maximum resolution on the order of 200, and a peak width of 0.6 amu [18]. Overall, the size and performance of the μGripper quadrupoles compares favorably with other small-scale quadrupoles, but with the added advantage of being cost effective and flexible. The current capabilities of the reported device will find applications where the low-cost detection of known substances is desired.

VI. Conclusion

Out-of-plane quadrupole mass filters that implement MEMS 3-D packaging technology were reported with assembled devices demonstrating a minimum peak width of 0.4 amu and a maximum mass range of 650 amu. Quadrupoles with rod diameters ranging from 1.58 to 0.25 mm have been constructed, and devices with rod diameter as small as 1.0 mm have been driven, establishing the μGripper technology as a low-cost option for miniaturized mass filters. The first mass spectrum of a MEMS quadrupole operated in the second stability region is provided, illustrating a potential strategy for improving the performance of small-scale quadrupoles. The ultimate resolution of the quadrupole technology reported makes a case for utilizing the ratio between the rod diameter and the precision of the assembly as a first-order estimate.

Appendix
Quadrupole Capacitance

Boumsellek and Ferran [9, p. 634] argued that as quadrupoles get smaller, their capacitance gets larger, but a simple 2-D model shows otherwise. The model assumes ideal quadrupole electric potentials established by hyperbolic electrode surfaces that are truncated in the orthogonal directions at a distance $D + r_{\rm o}$, where $D = 2 \cdot (\Psi \cdot r_{\rm o})$ with $r_{\rm o}$ being the aperture radius and Ψ the $r - to - r_{\rm o}$ ratio of the quadrupole. From Gauss' law, the charge on the electrode surface is

$$Q = \varepsilon_{\rm o} \oint \vec{E} \cdot d\vec{A} \tag{A1}$$

where $\varepsilon_{\rm o}$ is the permittivity of free space, $d\vec{A}$ is the normal area differential, and $\vec{E}$ is the electric field. Taking the Gaussian loop to be along the surfaces of the truncated electrode, the electric field along the hyperbolic surfaces is

$$\vec{E} = -\vec{\nabla}\phi = -\frac{\phi_{\rm o}}{r_{\rm o}^2}(x\hat{x} - y\hat{y})\Big|_{x^2-y^2=r_{\rm o}^2} \tag{A2}$$

with field lines parallel to $d\vec{A}$, and assumed to be zero on the truncated surfaces. Using these assumptions, the proposed limits, and symmetry arguments, the total capacitance of a quadrupole with aspect ratio k and length $L = kD$ is

$$\begin{aligned} C_{\rm o} &= \frac{4\varepsilon_{\rm o}L}{r_{\rm o}^2} \int_{x=r_0}^{x=(2\psi+1)r_{\rm o}} \frac{2x^2 - r_{\rm o}^2}{\sqrt{x^2 - r_{\rm o}^2}} dx \\ &= \frac{4\varepsilon_{\rm o}L}{r_{\rm o}^2} \left[x\sqrt{x^2 - r_{\rm o}^2}\right]\Big|_{x=r_{\rm o}}^{x=(2\psi+1)r_{\rm o}} \\ &= \left[8(2\psi+1)\sqrt{\psi^2+\psi}\right] \varepsilon_{\rm o} k D. \end{aligned} \tag{A3}$$

The model predicts that the capacitance scales with the rod diameter for a fixed aspect ratio. More importantly, the capacitance per unit length of quadrupoles should be a constant which was verified using Maxwell 2-D from Ansoft. Quadrupole cross sections with $\Psi = 1.148$ and $r_{\rm o}$ ranging between 50 and 500 μm were simulated with an energy error $< 0.1\%$. The

capacitance per unit length from Maxwell is 2.1 pF/cm, while the result from (A3) is 3.67 pF/cm. These values are overestimates because they neglect 3-D effects present in quadrupoles of finite length. A series of simulations using Maxwell 3-D was conducted to get a better estimate of the actual capacitance. Electrode diameters ranging from 500 to 1500 μm, and lengths between 25 and 100 mm were simulated with an energy error $< 5\%$. The average capacitance per unit length was 1.75 pF/cm, and was found to be nearly constant for quadrupoles with aspect ratios greater than 50. The measured capacitance of the MEMS quadrupoles reported in this paper was about 1.67 pF/cm.

ACKNOWLEDGMENT

The authors would like to thank the staff at MIT's Microsystems Technology Laboratories for the help during the microfabrication of the quadrupole platforms. The authors would also like to thank Dr. R. Pedder (Ardara Technologies, Ardara PA) for the decisive insights while performing the experimental characterization of the quadrupoles.

REFERENCES

[1] W. Paul and H. Steinwedel, "Ein neues Massenspektrometer ohne Magnetfeld," *Zeitschrift für Naturforschung*, vol. A8, no. 7, pp. 448–450, 1953.

[2] B. Ghodsian, M. Parameswaran, and M. Syrzycki, "Gas detector with low-cost micromachined field ionization tips," *IEEE Electron Device Lett.*, vol. 19, no. 7, pp. 241–243, Jul. 1998.

[3] S. C. Terry, J. H. Jerman, and J. B. Angell, "A gas chromatographic air analyzer fabricated on a silicon wafer," *IEEE Trans. Electron Devices*, vol. ED-26, no. 12, pp. 1880–1886, Dec. 1979.

[4] R. R. Reston and E. S. Kolesar, "Silicon-micromachined gas chromatography system used to separate and detect ammonia and nitrogen dioxide—Part I: Design, fabrication, and integration of the gas chromatography system," *J. Microelectromech. Syst.*, vol. 3, no. 4, pp. 134–146, Dec. 1994.

[5] R. T. Short, D. P. Fries, M. L. Kerr, and R. H. Byrne, "Field chemical analysis using real-time in-water mass spectrometry," in *Proc. IEEE Conf. Exhib. Oceans*, Sep. 2000, vol. 1, pp. 605–609.

[6] R. R. Reston and E. S. Kolesar, "Miniature gas chromatography system realized using conventional VLSI fabrication techniques applied to quantifying toxic environmental pollutants," in *Proc. IEEE NAECON*, May 1994, vol. 1, pp. 327–333.

[7] W. C. Wang, "Micromechanical devices at JPL for space exploration," in *Proc. IEEE Aerosp. Conf.*, 1998, vol. 1, pp. 461–470.

[8] P. M. Holland, A. Chutjian, M. R. Darrach, O. J. Orient, and D. Karmon, "Miniaturized GCMS instrumentation for in situ measurements: Micro gas chromatography coupled with miniature quadrupole array and Paul ion trap mass spectrometers," *Proc. SPIE*, vol. 4878, pp. 1–7, 2003.

[9] S. Boumsellek and R. J. Ferran, "Trade-offs in miniature quadrupole designs," *J. Amer. Soc. Mass Spectrom.*, vol. 12, no. 6, pp. 633–640, Jun. 2001.

[10] J. R. Gibson and S. Taylor, "Numerical investigation of the effect of electrode size on the behavior of quadrupole mass filters," *Rapid Commun. Mass Spectrom.*, vol. 15, pp. 1960–1964, 2001.

[11] A. Chutjian, M. R. Darrach, V. Garkanian, S. P. Jackson, T. D. Molsberry, O. Orient, D. Karmon, P. M. Holland, and D. Aalami, "A miniature quadrupole mass spectrometer array and GC for space flight: Astronaut EVA and cabin-air monitoring," SAE, Warrendale, PA, SAE Technical Paper Series 2000-01-2300, 2000.

[12] O. J. Orient, A. Chutjian, and V. Garkanian, "Miniature, high-resolution, quadrupole mass-spectrometer array," *Rev. Sci. Instrum.*, vol. 68, no. 3, pp. 1393–1397, Mar. 1997.

[13] D. H. Holkeboer, T. L. Karandy, F. C. Currier, L. C. Frees, and R. E. Ellefson, "Miniature quadrupole residual gas analyzer for process monitoring at milliTorr pressures," *J. Vac. Sci. Technol. A, Vac. Surf. Films*, vol. 16, no. 3, pp. 1157–1162, May 1998.

[14] R. J. Ferran and S. Boumsellek, "High-pressure effects in miniature arrays of quadrupole analyzers for residual gas analysis from 10^{-9} to 10^{-2} Torr," *J. Vac. Sci. Technol. A, Vac. Surf. Films*, vol. 14, no. 3, pp. 1258–1265, May 1996.

[15] S. Taylor, J. J. Tunstall, R. R. A. Syms, T. J. Tate, and M. M. Ahmad, "Initial results for a quadrupole mass spectrometer with a silicon micromachined mass filter," *Electron. Lett.*, vol. 34, no. 6, pp. 546–547, Mar. 1998.

[16] R. Syms, T. J. Tate, M. M. Ahmad, and S. Taylor, "Design of a microengineered electrostatic quadrupole lens," *IEEE Trans. Electron Devices*, vol. 45, no. 11, pp. 2304–2311, Nov. 1998.

[17] S. Taylor, J. J. Tunstall, J. H. Leck, R. Tindall, P. Julian, J. Batey, R. R. A. Syms, T. J. Tate, and M. M. Ahmad, "Performance improvements for a miniature quadrupole with a micromachined mass filter," *Vacuum*, vol. 53, no. 1/2, pp. 203–206, May 1999.

[18] M. Geear, R. R. A. Syms, S. Wright, and A. S. Holmes, "Monolithic MEMS quadrupole mass spectrometers by deep silicon etching," *J. Microelectromech. Syst.*, vol. 14, no. 5, pp. 1156–1166, Oct. 2005.

[19] G. F. Verbeck, R. Saini, J. W. Wylde, K. Tsui, and M. Ellis, "MEMS assembled mass spectrometry: A novel approach to miniaturization and construction of electron and ion optics," in *Proc. 54th ASMS Conf. Mass Spectrometry*, Seattle, WA, 2006.

[20] N. Sillon and R. Baptist, "Micromachined mass spectrometer," *Sens. Actuators B, Chem.*, vol. 83, no. 1/3, pp. 129–137, Mar. 2002.

[21] D. Wiberg, N. V. Myung, B. Eyre, K. Shcheglov, O. Orient, E. Moore, and P. Munz, "LIGA fabricated two-dimensional quadrupole array and scroll pump for miniature gas chromatograph/mass spectrometer," *Proc. SPIE*, vol. 4878, pp. 8–13, 2003.

[22] L.-Y. Chen, L. F. Velasquez-Garcia, X. Wang, K. Teo, and A. I. Akinwande, "A micro ionizer for portable mass spectrometers using double-gated isolated vertically aligned carbon nanofiber arrays," in *IEDM Tech. Dig.*, Washington, DC, Dec. 2007, pp. 843–846.

[23] Y. Zhu, J. Lee, and A. Seshia, "System-level simulation of a micromachined electrometer using a time-domain variable capacitor circuit model," *J. Micromech. Microeng.*, vol. 17, no. 5, pp. 1059–1065, May 2007.

[24] L. F. Velásquez-García, A. I. Akinwande, and M. Martínez-Sánchez, "Precision hand assembly of MEMS subsystems using DRIE-patterned deflection spring structures: An example of an out-of-plane substrate assembly," *J. Microelectromech. Syst.*, vol. 16, no. 3, pp. 598–612, Jun. 2007.

[25] P. Dawson, *Quadrupole Mass Spectrometry and Its Applications*. College Park, MD: AIP, 1997.

[26] F. M. Mao and J. H. Leck, "The quadrupole mass spectrometer in practical operation," *Vacuum*, vol. 37, no. 8/9, pp. 659–668, 1987.

[27] W. C. Elmore and M. W. Garret, "The measurement of two-dimensional fields. Part I: Theory," *Rev. Sci. Instrum.*, vol. 25, no. 5, pp. 480–485, May 1954.

[28] I. E. Dayton, F. C. Shoemaker, and R. F. Mozley, "The measurement of two-dimensional fields. Part II: Study of a quadrupole magnet," *Rev. Sci. Instrum.*, vol. 25, no. 5, pp. 485–489, May 1954.

[29] D. R. Denison, "Operating parameters of a quadrupole in a grounded cylindrical housing," *J. Vac. Sci. Technol. A, Vac. Surf. Films*, vol. 8, no. 1, pp. 266–269, Jan./Feb. 1971.

[30] D. J. Douglas and N. V. Konenkov, "Influence of the 6th and 10th spatial harmonics on the peak shape of a quadrupole mass filter with round rods," *Rapid Commun. Mass Spectrom.*, vol. 16, no. 15, pp. 1425–1431, Aug. 2002.

[31] T. J. Hogan and S. Taylor, "Performance simulation of a quadrupole mass filter operating in the first and third stability zones," *IEEE Trans. Instrum. Meas.*, vol. 57, no. 3, pp. 498–508, Mar. 2008.

[32] J. R. Gibson and S. Taylor, "Prediction of quadrupole mass filter performance for hyperbolic and circular cross section electrodes," *Rapid Commun. Mass Spectrom.*, vol. 14, no. 18, pp. 1669–1672, Sep. 2000.

[33] Z. Du, D. J. Douglas, and N. Konenkov, "Elemental analysis with quadrupole mass filters operated in higher stability regions," *J. Anal. At. Spectrom.*, vol. 14, no. 8, pp. 1111–1119, 1999.

[34] P. H. Dawson, "Higher zones of stability for the quadrupole mass filter," *J. Vac. Sci. Technol.*, vol. 11, no. 6, pp. 1151–1153, Nov. 1974.

[35] J. R. Taylor, *An Introduction to Error Analysis: The Study of Uncertainties in Physical Measurements*. Herndon, VA: Univ. Sci. Books, 1982, p. 73.

[36] B. Gassend, L. F. Velásquez-García, and A. I. Akinwande, "Precision in-plane hand assembly of bulk-microfabricated components for high voltage MEMS arrays applications," *J. Microelectromech. Syst.*, 2008. submitted for publication.

[37] L. F. Velásquez-García and A. I. Akinwande, "An out-of-plane MEMS quadrupole for a portable mass spectrometer," in *Proc. Tech. Dig. 14th Int. Conf. Solid-State Sensors, Actuators Microsyst.*, Lyon, France, 2007, vol. 2, pp. 2315–2320.

[38] R. Pedder, "Practical Quadrupole Theory: Graphical Theory," Excel Core Mass Spectrometers, Pittsburgh, PA, Extrel Application Note RA_2010 A, 2001.
[39] J. R. Gibson and S. Taylor, "Asymmetrical features of mass spectral peaks produced by quadrupole mass filters," *Rapid Commun. Mass Spectrom.*, vol. 17, no. 10, pp. 1051–1055, May 2003.
[40] V. V. Titov, "Detailed study of the quadrupole mass analyzer operating within the first, second, and third (intermediate) stability regions. II. Transmission and resolution," *J. Amer. Soc. Mass Spectrom.*, vol. 9, no. 1, pp. 70–87, Jan. 1998.
[41] R. Pedder, Ardara Technol., Ardara, PA, personal communication.

Luis F. Velásquez-García received the BS degree in mechanical engineering (valedictorian of the School of Engineering, magna cum laude) and the BS degree in civil engineering (valedictorian of the School of Engineering, magna cum laude) from the Universidad de Los Andes, Bogotá, Colombia, in 1998 and 1999, respectively, and the M.S. degree in aeronautics and astronautics and the Ph.D. degree in space propulsion from the Massachusetts Institute of Technology (MIT), Cambridge, in 2001 and 2004, respectively.

In 2004, after completing his studies, he became a Postdoctoral Associate with the Microsystems Technology Laboratories, MIT, where he has been a Research Scientist since 2005. His research focuses on the application of microfabrication and nanofabrication technologies to propulsion, analytical, and power systems. He has conducted research in microtechnology and nanotechnology applied to electrospray arrays, carbon-nanotube-based devices, 3-D packaging, mass spectrometry, propulsion, and chemical reactors.

Dr. Velásquez-García is a member of the Honor Society of Science and Engineering (Sigma Xi).

Kerry Cheung received the B.S. degree in applied and engineering physics from Cornell University, Ithaca, NY, in 2003 and the M.S. degree in electrical engineering from the Massachusetts Institute of Technology (MIT), Cambridge, in 2005. He is currently working toward the Ph.D. degree in the Department of Electrical Engineering and Computer Science, MIT.

His research interests are in MEMS devices for mass spectroscopy and microfabrication technologies.

Akintunde I. Akinwande received the B.Sc. degree in electrical and electronic engineering from the University of Ife, Ife, Nigeria, in 1978 and the M.S. and Ph.D. degrees in electrical engineering from Stanford University, Stanford, CA, in 1981 and 1986, respectively.

He joined Honeywell Inc. in 1986, where he initially conducted research on GaAs complementary FET technology for very high speed and low-power signal processing. He later joined the Si Microstructures Group, where he conducted research on pressure sensors, accelerometers, thin-film field emission and display devices. He is currently a Professor in the Electrical Engineering and Computer Science Department, Massachusetts Institute of Technology (MIT), Cambridge. He joined the Microsystems Technology Laboratories, MIT, in January 1995, where his research focuses on microfabrication and electronic devices, with particular emphasis on smart sensors and actuators, intelligent displays, large-area electronics (macroelectronics), field emission and field ionization devices, mass spectrometry, and electric propulsion. He was a Visiting Professor in the Department of Engineering and an Overseas Fellow of Churchill College at the University of Cambridge, Cambridge, U.K., from 2002 to 2003. He is the author of more than 100 journal publications. He is the holder of numerous patents in MEMS, electronics on flexible substrates, display technologies.

Prof. Akinwande is a recipient of the 1996 National Science Foundation Career Award. He is a current member of the IEEE Nanotechnology Council. He has served a number of technical program committees for various conferences, including the Device Research Conference, the International Electron Devices Meeting, the International Solid-State Circuits Conference, the International Display Research Conference, and the International Vacuum Microelectronics Conference.